Title

The Streptococcus pyogenes Shr protein captures human hemoglobin using two structurally unique binding domains

Journal

Journal of Biological Chemistry, 293(47)

ISSN

0021-9258

Authors

Macdonald, Ramsay
Cascio, Duilio
Collazo, Michael J
et al.

Publication Date

2018-11-01

DOI

10.1074/jbc.ra118.005261

Peer reviewed

The *Streptococcus pyogenes* Shr protein captures human hemoglobin using two structurally unique binding domains

Received for publication, August 10, 2018, and in revised form, October 3, 2018 Published, Papers in Press, October 9, 2018, DOI 10.1074/jbc.RA118.005261

Ramsay Macdonald[‡§1], **Duilio Cascio**[§], **Michael J. Collazo**[§], **Martin Phillips**[‡], **and Robert T. Clubb**[‡§¶2]

From the [‡]*Department of Chemistry and Biochemistry,* [§]*UCLA-DOE Institute of Genomics and Proteomics and* [¶]*Molecular Biology Institute, UCLA, Los Angeles, California 90095*

Edited by Wolfgang Peti

In order to proliferate and mount an infection, many bacterial pathogens need to acquire iron from their host. The most abundant iron source in the body is the oxygen transporter hemoglobin (Hb). *Streptococcus pyogenes*, a potentially lethal human pathogen, uses the Shr protein to capture Hb on the cell surface. Shr is an important virulence factor, yet the mechanism by which it captures Hb and acquires its heme is not well-understood. Here, we show using NMR and biochemical methods that Shr binds Hb using two related modules that were previously defined as domains of unknown function (DUF1533). These hemoglobin-interacting domains (HIDs), called HID1 and HID2, are autonomously folded and independently bind Hb. The 1.5 Å resolution crystal structure of HID2 revealed that it is a structurally unique Hb-binding domain. Mutagenesis studies revealed a conserved tyrosine in both HIDs that is essential for Hb binding. Our biochemical studies indicate that HID2 binds Hb with higher affinity than HID1 and that the Hb tetramer is engaged by two Shr receptors. NMR studies reveal the presence of a third autonomously folded domain between HID2 and a heme-binding NEAT1 domain, suggesting that this linker domain may position NEAT1 near Hb for heme capture.

Streptococcus pyogenes (Group A *Streptococcus*) each year causes an estimated 700 million infections worldwide (1). Although most of these infections lead to nonlife-threatening acute pharyngitis, many are lethal and cause ~500,000 deaths annually (2). These more severe and invasive infections have a high mortality rate (~30%) and include necrotizing fasciitis and streptococcal toxic shock syndrome (3, 4). Infections caused by this deadly microbe are presently among the top 10 causes of death from an infectious disease worldwide (5). *S. pyogenes* and other pathogenic bacteria require iron to proliferate, as it is a versatile metal that functions as a key biocatalyst and electron carrier in enzymes that mediate metabolism (6). During infections, iron is frequently foraged from human hemoglobin (Hb),[3] which contains ~75–80% of the body's total iron content in the form of heme (iron–protoporphyrin IX). Recent studies have shown that *S. pyogenes* uses an array of surface and membrane-associated proteins to acquire Hb's heme. Understanding how these proteins function at a molecular level is of fundamental importance and could facilitate the discovery of new anti-infective agents that work by limiting microbial access to iron.

Surface and membrane-associated proteins are used by *S. pyogenes* to capture heme. The streptococcal hemoprotein receptor (Shr) is displayed on the bacterium's surface, where it binds to Hb and acquires the oxidized form of heme (called hemin) (7–11). The Shr Hb receptor is an important virulence factor, as Δ*shr* mutant strains of *S. pyogenes* exhibit reduced growth in human blood and attenuated virulence in murine and zebrafish models of infection (10, 12). *In vitro*, Shr transfers hemin directly to Shp, a cell wall–associated hemoprotein that uses a bis-methionine ligation mechanism to interact with hemin (13–15). Shp then passes hemin to HtsA/SiaA, the lipoprotein component of the ABC transporter HtsABC/SiaABC (16). A binary Shp–HtsA complex mediates this transfer step, in which the methionine axial ligands in Shp are displaced by methionine and histidine axial ligands within HtsA (17–21). This process occurs very rapidly, >100,000 times faster than the rate at which Shp spontaneously releases hemin into the solvent. Hemin is then presumably transported across the membrane into the bacterial cytoplasm where it is degraded by a yet to be identified oxygenase(s) that releases hemin's iron for use by the microbe (6). Although hemin transfer from Shp to HtsA/SiaA has been extensively studied by Lei and co-workers (20), the first step in the pathway, the extraction of hemin from human Hb by Shr, is less well-understood and the focus of this study.

Many Gram-positive bacterial pathogens display Hb receptors that contain near–iron transport (NEAT) domains (22, 23). NEAT domains have been shown to bind Hb, hemin, and in

This work was supported in part by National Science Foundation Grant MCB-1716948 and National Institutes of Health Grant AI052217. The authors declare that they have no conflicts of interest with the contents of this article. The content is solely the responsibility of the authors and does not necessarily represent the official views of the National Institutes of Health.

This article contains Figs. S1–S2 and Table S1.

The atomic coordinates and structure factors (code 6DKQ) have been deposited in the Protein Data Bank (http://wwpdb.org/).

Submitted to the BMRB Database under accession number 27550.

[1] Supported by National Institutes of Health Cellular and Molecular Biology Training Grant, Ruth L. Kirschstein NRSA GM007185.

[2] To whom correspondence should be addressed: Dept. of Chemistry and Biochemistry, UCLA, 602 Boyer Hall, 611 Charles Young Dr. East, Los Angeles, CA 90095. Tel.: 310-206-2334; Fax: 310-206-4749; E-mail: rclubb@mbi.ucla.edu.

[3] The abbreviations used are: Hb, hemoglobin; Shr, streptococcal hemoprotein receptor; HID, hemoglobin interacting domain; HSQC, heteronuclear single quantum coherence; SEC-MALS, size-exclusion chromatography with inline multiangle light scattering; ITC, isothermal titration calorimetry; AUC, analytical ultracentrifugation; CTR, C-terminal region; NTR, N-terminal region; PDB, Protein Data Bank; CV, column volume; r.m.s.d., root mean square deviation.

many instances are able to rapidly transfer hemin among one another (24–35). Hemin acquisition by *Staphylococcus aureus* has been studied extensively. This microbe uses an array of iron-regulated surface determinant (Isd) proteins that each contain one or more NEAT domains (24, 29, 36–40). Hb is captured on the cell surface by the closely related IsdB and IsdH proteins (41). Our studies have shown that IsdH captures and extracts hemin from Hb using a conserved tri-domain unit that contains two NEAT domains, called N2 and N3, that are separated by a helical linker domain (42). As compared with the rate of hemin released into the solvent by Hb, binding of the tri-domain unit accelerates hemin release 13,400-fold (43). Atomic structures of IsdH–Hb complexes reveal that its N2 and N3 NEAT domains adopt related β-sandwich structures that are decorated by short helices, whereas the intervening linker domain adopts a three-helix bundle (44, 45). The N2 domain engages Hb's A-helix with high affinity, enabling the helical and N3 domains to distort Hb's F-helix, thereby promoting hemin transfer to IsdH's N3 domain (43, 45, 46). IsdB shares significant primary sequence homology with IsdH and also contains a tri-domain unit that captures hemin from Hb through a similar mechanism (31, 34, 42, 47–50). Other Gram-positive pathogens use NEAT domains to bind hemin and/or Hb, and include among others *Listeria monocytogenes*, *Bacillus anthracis*, *Bacillus cereus*, and *S. pyogenes* (23). However, the mechanisms used by these domains to capture hemin from Hb may be distinct from that in IsdH and IsdB, because in some instances a single NEAT domain has been proposed to bind to both Hb and heme (51–54). Notable examples are IsdX1, IsdX2, and Hal in which single NEAT domains from these proteins have been reported to bind Hb and extract hemin from Hb (52–54). However, complexes of these NEAT domains bound to Hb have not been visualized at atomic resolution.

Unlike other Hb receptors in Gram-positive bacteria, the *S. pyogenes* Shr protein does not use NEAT domains to engage Hb. Instead, it binds Hb via an N-terminal region (NTR) that is predicted to contain two domains of unknown function, called DUF1533 domains (Fig. 1) (8, 11). Released hemin is then bound by residues located within Shr's C-terminal region (CTR) (residues 365–1275), which contains two hemin-binding NEAT domains (NEAT1 and NEAT2) that are separated from one another by a series of leucine-rich repeats (8). Interestingly, similar to the staphylococcal IsdB and IsdH proteins, transfer experiments have shown that the isolated Shr protein increases the rate of hemin release from Hb *in vitro*, suggesting that the domains within the receptor function synergistically to extract hemin (9). The NEAT domains within Shr can rapidly transfer hemin among one another, but only NEAT1 is able to efficiently transfer hemin to Shp (55). These findings led to the suggestion that NEAT2 stores hemin near the cell surface (55).

Here, we show that Shr uses two related DUF1533 domains to engage Hb, which we rename Hb-interacting domains (HIDs). Biochemical studies and the atomic structure of a HID reveal that it is a structurally novel Hb-binding module that employs a conserved tyrosine residue for Hb recognition. Biochemical studies indicate that the HIDs within Shr bind Hb with differing affinities and suggest that each engages a single globin subunit. Interestingly, NMR studies reveal the presence of a third autonomously folded domain that is located between the HID2 and NEAT1 domains. The implications of this arrangement in hemin acquisition from Hb are discussed.

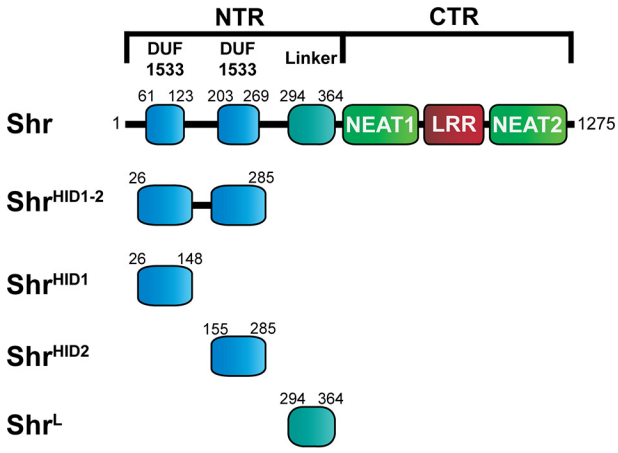

Figure 1. Domain arrangement within Shr and the protein constructs used in this study. The *Top panel* shows the domains that have been identified in Shr. Previous studies have shown that Shr contains an Hb-binding NTR and a hemin-binding CTR. Polypeptides used in this study contain regions within the NTR and include: Shr^{HID1} and Shr^{HID2} that contain the first and second DUF1533 domains (renamed HIDs), respectively; Shr^{L}, which is predicted to contain several α-helices; and Shr^{HID1-2}, which contains both of the DUF1533 domains. The DUF1533 domains are HIDs based on findings reported in this paper.

Results

Hb-interacting N-terminal region within Shr contains three autonomously folded domains

Previous studies have shown the *S. pyogenes* Shr protein interacts with Hb via residues located at its N terminus (8). This N-terminal region is formed by residues Lys-25–Val-364 and is hereafter referred to as the NTR (Fig. 1). An inspection of its primary sequence suggests that the NTR contains three folded regions. These include two domains of unknown function (DUF1533 domains) that are formed by residues Gly-61–Phe-123 and Ile-203–Val-269 (8), as well as residues Val-299–Ser-358 that are predicted to form several α-helices. Constructs containing residues Gly-61–Phe-123 and Ile-203–Val-269 were insoluble. Secondary structural prediction algorithms such as PSIPRED (56) and JPred (57) were used to guide the design of additional constructs until highly soluble ones were obtained and characterized by NMR: Shr^{HID1}, residues Ser-26–Lys-148 that correspond to the first DUF1533 domain; Shr^{HID2}, residues Lys-155–Gln-285 that correspond to the second DUF1533 domain; and Shr^{L}, residues Ser-294–Val-364 that contain the predicted α-helical region in Shr that links Shr^{HID2} to the first NEAT domain (Fig. 1). In each case, constructs included at least two residues beyond the predicted secondary structure elements at both the N and C termini. If ambiguous, extra residues were included to ensure that no potentially important structural elements were truncated. Each polypeptide was uniformly ^{15}N-labeled and purified, and its ^{1}H–^{15}N HSQC spectrum was recorded (Fig. 2, *a, c,* and *e*). All three polypeptides adopt a folded structure, as the cross-peaks in each spectrum are well-dispersed and have appropriate line

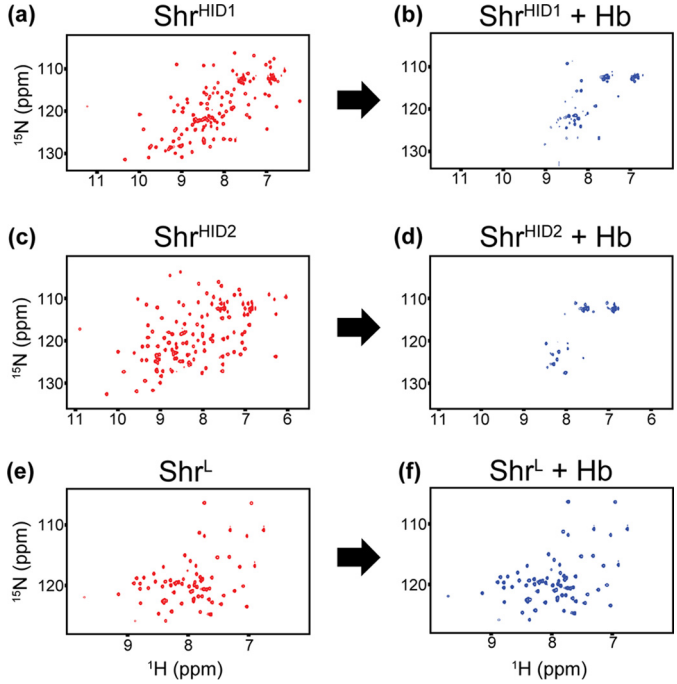

Figure 2. Hb binding studies by NMR. Panels showing the $^{1}H–^{15}N$ HSQC spectra of Shr proteins in the presence and absence of Hb. *a* and *b* show the $^{1}H–^{15}N$ HSQC spectra [^{15}N]Shr^{HID1} in the presence and absence of Hb (1:1 molar equivalent in tetramer units), respectively. *c* and *d* show the $^{1}H–^{15}N$ HSQC spectra [^{15}N]Shr^{HID2} in the presence and absence of Hb (1:1 molar equivalent in tetramer units), respectively. *e* and *f* show the $^{1}H–^{15}N$ HSQC spectra [^{15}N]Shr^{L} in the presence and absence of Hb (1:1 molar equivalent in tetramer units), respectively. Only polypeptides containing the DUF1533 domains interact with Hb.

widths. Based on the Pfam prediction for their domain boundaries, the two DUF1533 domains within the NTR are separated by ~80 amino acids. To determine whether the domains interact with one another, a longer polypeptide fragment containing both domains was characterized by NMR (Shr$^{HID1–2}$, consisting of residues Ser-26–Gln-285). Superposition of the NMR spectra of [^{15}N]Shr^{HID1} and [^{15}N]Shr^{HID2} onto the spectrum of [^{15}N]Shr$^{HID1–2}$ reveals that the cross-peaks have similar chemical shifts (Fig. S1). Thus, in the context of the longer Shr$^{HID1–2}$ polypeptide, the Shr^{HID1} and Shr^{HID2} domains do not significantly interact with one another, and they exhibit the same structural fold as they do in isolation. The Shr^{HID2} and Shr^{L} domains also do not interact with one another, as the NMR spectra of a polypeptide containing both of these domains ([^{15}N]Shr^{HID2-L}, residues Gly-61–Asn-368) can be recapitulated by summing the spectra of the isolated [^{15}N]Shr^{HID2} and [^{15}N]Shr^{L} domains (Fig. S1). We conclude from the NMR data that the Hb-interacting region within Shr contains three independently folded and noninteracting structural domains, two DUF1533 domains, and a linker domain that is predicted to contain several α-helices.

DUF1533 domains bind Hb

We used NMR to determine whether the domains within the NTR interacted with Hb. The $^{1}H–^{15}N$ HSQC spectrum of each ^{15}N-labeled domain was recorded in the presence or absence of Hb (1:1 stoichiometry based on tetramer units) (Fig. 2). Upon adding Hb to a solution containing [^{15}N]Shr^{HID1}, a massive loss of signal occurs indicative of complex formation. This is caused by increased T_2 relaxation that occurs because of the significantly larger molecular weight of the complex, and possibly as a result of intermediate conformational exchange on the chemical shift time scale. A similar result is obtained when Hb was added to [^{15}N]Shr^{HID2} (Fig. 2, compare *a* and *c* with *b* and *d*), indicating that both DUF1533 domains interact with Hb. In contrast, adding Hb to the [^{15}N]Shr^{L} domain causes only minimal changes in the NMR spectrum indicating that the proteins do not interact (Fig. 2*f*).

Having established that DUF1533 domains bind to Hb, we next measured their affinities using ITC (Fig. 3, *a–d*, and Table 1). These data indicate that Shr^{HID2} binds Hb with a K_D = 16.0 ± 3.4 μM in a process that is enthalpically favorable (Fig. 3*b* and Table 1). Shr^{HID1} also binds Hb, but the interaction is weaker (K_D = ~140 μM). The Shr$^{HID1–2}$ polypeptide containing both DUF1533 domains binds Hb with a K_D = 5.1 ± 0.4 μM (Fig. 3*a* and Table 1). Considering that the binding parameters for Shr$^{HID1–2}$ are distinct from either HID domain in isolation, it seems likely that Shr$^{HID1–2}$ exhibits binding avidity. If HID1 and HID2 were binding completely independently, one would expect the Shr$^{HID1–2}$–Hb binding parameters to more closely resemble the higher affinity Shr^{HID2}–Hb interaction. From these data, we conclude that both of Shr's DUF1533 domains bind Hb, and the second domain (Shr^{HID2}) is the most important for binding. Based on these results, we propose that the DUF1533 domains within Shr be renamed hemoglobin interacting domains (HIDs).

A NMR experiment was performed to ascertain whether the HIDs (DUF1533 domains) bind to the same site on Hb. In this experiment, the ability of unlabeled Shr^{HID2} to displace Hb-bound [^{15}N]Shr^{HID1} was determined. Initially, unlabeled Hb was titrated into a solution of [^{15}N]Shr^{HID1} such that the signals in its $^{1}H–^{15}N$ HSQC spectrum were broadened beyond detection as a result of complex formation (Fig. 4*b*). Unlabeled Shr^{HID2} was then titrated into the solution, and the $^{1}H–^{15}N$ HSQC spectrum was recorded to determine whether it displaces [^{15}N]Shr^{HID1} from Hb. Adding unlabeled Shr^{HID2} to the solution causes the signals from [^{15}N]Shr^{HID1} to reappear in the HSQC spectrum, meaning that Shr^{HID2} outcompetes [^{15}N]Shr^{HID1} for its binding site(s) located on Hb. The data show a progressive reappearance of the signals from [^{15}N]Shr^{HID1}, starting when a 2-fold molar equivalent of Shr^{HID2} is added (Fig. 4*c*). When 4-fold Shr^{HID2} is added, the spectrum of [^{15}N]Shr^{HID1} is almost completely recovered, yet the signal intensities are approximately one-third as intense as in the original HSQC (Fig. 4*d*). Importantly, the reappearance of the NMR signals is not caused by simply diluting the NMR sample, as the signals from [^{15}N]Shr^{HID1} remain broadened in a control experiment in which the [^{15}N]Shr^{HID1}–Hb complex was diluted only with buffer. As unlabeled Shr^{HID2} displaces [^{15}N]Shr^{HID1} from Hb, we conclude that the isolated domains can compete for the same site(s) on Hb. However, the fact that this resulted in only a partial recovery of signal could indicate that Shr^{HID1} binds a second site on Hb and binds to Hb more promiscuously than Shr^{HID2}.

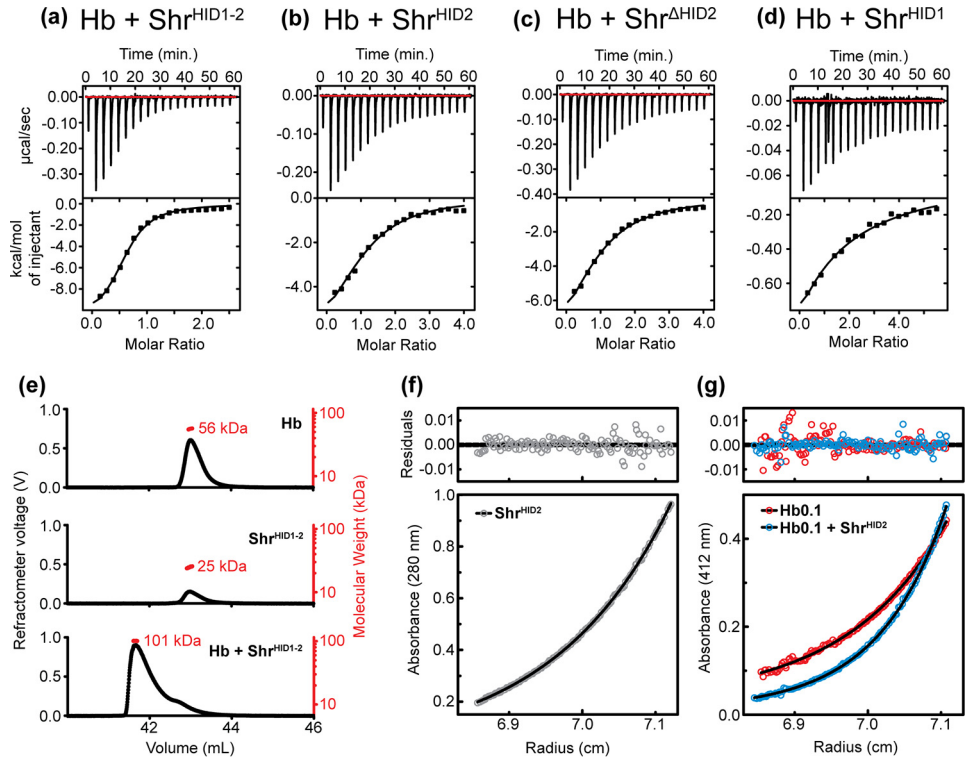

Figure 3. Biochemical studies of Hb binding. *a–d* show representative ITC Hb binding data for Shr^{HID1-2} (*a*), Shr^{HID2} (*b*), $Shr^{\Delta HID2}$ (*c*), and Shr^{HID1} (*d*). In each titration experiment, Shr polypeptides were injected into a cell containing Hb. In each panel, at the *top* is shown the time course of the titration (*black*) and baseline (*red*). The *bottom part* of the panel shows the integrated isotherms (*squares*) and the curve fit (*line*). As is standard, the first data point in each experiment was eliminated prior to analysis. The fifth data point in the Shr^{HID1} titration was also eliminated due to a spurious double peak. Origin software was used to analyze the data. *e,* SEC-MALS data defining receptor–Hb interactions. Elution profiles of Hb alone, Shr^{HID1-2} alone, and Hb in combination with Shr^{HID1-2}. Refractometer voltage is indicated on the left *y* axis, and the corresponding trace is shown in *black*. The elution volume is shown on the *x* axis. ASTRA software was used to analyze the data. The molecular weight is indicated on the right *y* axis. Interestingly, the measured Hb molecular weight is slightly smaller than its predicted molecular mass of 64.5 kDa based on its primary sequence, a discrepancy that has also been observed by others (65, 66). *f* and *g*, sedimentation equilibrium data defining receptor–Hb interactions. The panel shows profiles of Shr^{HID2} alone (*gray*) at 26,000 rpm, as well as Hb alone (*red*) and in complex with Shr^{HID2} (*blue*) at a 1:45 ratio of Hb0.1 (heme basis)/Shr^{HID2} at 13,000 rpm. The *top panels* show the residuals of the fit of the experimental data, and the *bottom panels* show the absorbance readings on the *y* axis *versus* the radial position on the *x* axis. *Circles* and *curved black lines* correspond to experimental data and calculated fits to binding models described in the text, respectively.

Table 1

Thermodynamic parameters and affinity data for Hb binding

Errors represent the standard deviation of three replicates.

	K_D	ΔH^0	ΔS^0	ΔG^{0a}	n^b
	µM	*kcal/mol*	*cal/mol·K*	*kcal/mol*	
Hb + Shr^{HID1-2}	5.1 ± 0.4	−13.2 ± 1.1	−19.9 ± 3.9	−7.2 ± 0.1	0.58 ± 0.03
Hb + Shr^{HID2}	16.0 ± 3.4	−7.8 ± 1.0	−4.3 ± 3.6	−6.6 ± 0.1	1.06 ± 0.08
Hb + $Shr^{\Delta HID2}$	20.8 ± 0.7	−9.2 ± 1.1	−9.5 ± 3.7	−6.4 ± 0.1	1.14 ± 0.14
Hb + Shr^{HID1}	~143	ND[c]	ND	ND	ND

[a] Samples were in buffer containing 20 mM sodium phosphate, 150 mM NaCl, 450 mM sucrose, pH 7.5, 298 K.
[b] *n* refers to the molar ratio protein/Hb.
[c] ND refers to "not determined."

Two Shr^{HID1-2} proteins bind to tetrameric Hb

The binding stoichiometry of the Shr^{HID1-2}–Hb complex was determined using size-exclusion chromatography with inline multiangle light scattering (SEC-MALS). When Shr^{HID1-2} is mixed with the Hb tetramer at a ratio of 2:1 (Shr^{HID1-2} to Hb tetramer units), a complex at 101 kDa is observed (Fig. 3*e*). This is consistent with ~1.8 Shr^{HID1-2} proteins binding to one Hb tetramer (calculated as follows: (101 $kDa_{(complex)}$ − 56 $kDa_{(Hb\ alone)}$)/25 $kDa_{(Shr^{HID1-2}\ alone)}$ = 1.8). SEC-MALS experiments using higher Shr^{HID1-2}/Hb ratios (4:1 and 6:1) were also performed and yielded similar results, indicating that Hb is saturated, and a maximum of two Shr^{HID1-2} proteins bind to one Hb tetramer. Notably, the stoichiometry predicted by SEC-MALS is similar to that obtained from curve-fitting of the ITC data (Table 1); two Shr^{HID1-2} proteins bind to one Hb tetramer.

Analytical ultracentrifugation (AUC) was used to determine the stoichiometry of the Shr^{HID2}–Hb complex. This method was used instead of SEC-MALS because the molecular weights of Hb and its complex with Shr^{HID2} are too similar, making it difficult to resolve these species by column chromatography. Similar to Shr^{HID1-2}, Shr^{HID2} is monomeric in solution (Fig. 3*f*); it has a weighted average molecular weight of 13.3 kDa (Table S1), which corresponds closely to its theoretical molecular weight of 14.4 kDa (58). To simplify the analysis of the AUC data, binding experiments employed Hb0.1, a stabilized tetra-

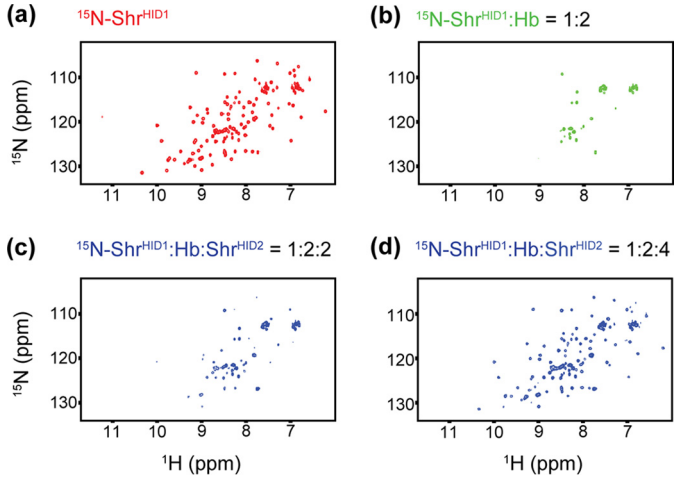

Figure 4. Hb binding competition experiment. NMR was used to demonstrate that the isolated HIDs domain can compete for the same site on Hb. Data are similar to that shown in Fig. 2. The *panels* show the ^{1}H–^{15}N HSQC spectra of [^{15}N]Shr^{HID1}. *a* shows the spectrum of the [^{15}N]Shr^{HID1} protein in isolation, and *b* shows its spectrum in the presence of 2-fold excess of Hb (heme basis). *c* and *d* are similar to *b*. They show the spectrum of a 2:1 (*c*) and a 4:1 (*d*) equivalent of unlabeled Shr^{HID2}/[^{15}N]Shr^{HID1} to the sample.

meric from of Hb in which the α-globin chains are part of a single polypeptide. When Shr^{HID2} is added to Hb0.1 at a 180-fold molar excess (Hb tetramer units), its weighted average molecular mass is 97.4 kDa (Fig. 3*g* and Table S1), consistent with two Shr^{HID2} domains binding to one Hb0.1 tetramer. Hb0.1 is saturated with Shr^{HID2}, because similar molecular weights are measured when Shr^{HID2} is present at 60-fold molar excess. Interestingly, the binding stoichiometry obtained from fitting the ITC data suggests that four Shr^{HID2} proteins can bind to a tetramer, which differs from the 2:1 stoichiometry determined by AUC (Table 1). The origin of this discrepancy is unclear, but it may result from the different conditions employed in each experiment.

HID is a structurally novel Hb-binding domain

To gain insight into the molecular basis of Hb binding, we determined the crystal structure of HID2, the second DUF1533 domain within Shr. To facilitate its crystallization, we first used NMR to delineate regions within the Shr^{HID2} polypeptide that are structurally ordered. Triple resonance methods were applied to [U-^{13}C,U-^{15}N]Shr^{HID2}, enabling ~94% of its backbone resonances to be assigned (Fig. 5*a*). A heteronuclear {^{1}H}^{15}N NOE experiment was then performed to identify regions within Shr^{HID2} that are mobile and unstructured (Fig. 5*b*). The majority of residues within Shr^{HID2} are structurally ordered in the absence of Hb, as indicated by heteronuclear NOE values >0.6 for backbone amide groups that span residues Ile-179–Gln-283. However, ~20 residues located at the N terminus of Shr^{HID2} are disordered, as they possess low magnitude heteronuclear NOEs. We therefore produced a truncated variant of Shr^{HID2} for X-ray crystallography studies that removes its unstructured N-terminal residues Lys-155–Ala-174 yielding a new construct (Shr$^{\Delta HID2}$, residues Asn-175–Gln-285). Importantly, Shr$^{\Delta HID2}$ binds to Hb with similar affinity and stoichiometry as Shr^{HID2} (Fig. 3*c* and Table 1), indicating that the deleted N-terminal residues are not important for function.

The structure of Shr$^{\Delta HID2}$ was determined at 1.5 Å resolution using single-wavelength anomalous diffraction methods applied to native and KI-soaked crystals. Two Shr$^{\Delta HID2}$ domains are present in the asymmetric unit (Fig. 6*a*), forming a 2-fold symmetry-related dimer that buries 517 Å^2 of surface area (59). As SEC-MALS and AUC analyses indicate that Shr$^{\Delta HID2}$ is monomeric, the dimer observed in the structure is likely an artifact caused by the high concentration of protein present in the crystal. The two polypeptide chains in the dimer possess nearly identical atomic structures, as their heavy atom coordinates can be superimposed with a r.m.s.d. of 0.80 Å. The polypeptides are well-defined by the electron density, with the exception of residue Asp-226 in chain A and residues Lys-284 and Gln-285 in chain B. Complete structural and data statistics are presented in Table 2.

Shr$^{\Delta HID2}$ adopts a β-sandwich–type fold in which two antiparallel β-sheets are flanked by an α-helix. One face of the sandwich is formed by a sheet containing strands β1, β2, β6, and β5 (β-sheet 1), whereas the other face is formed by a sheet containing strands β9, β8, β7, β3, and β4 (β-sheet 2) (Fig. 6*b*). Strands β1 and β2 form an antiparallel β-hairpin. The β2 strand is then followed by a long loop that is connected to a two-turn α-helix that is positioned nearly perpendicular with respect to β-sheet 2. Following the helix, strand β3 makes antiparallel contacts with strand β7 in β-sheet 2. Strand β4 then forms part of a β-hairpin with β3 before being followed by an extended loop that winds around and extends over the top of β-sheet 1. This is followed by strand β5 that forms a β-hairpin with strand β6 and together with strands β1 and β2 comprise β-sheet 1. The structure is completed by a β-meander that is constructed from strands β7, β8, and β9 within β-sheet 2. Shr^{HID1} presumably adopts a similar structure, as it shares 27% sequence identity with Shr^{HID2}. The solvent-exposed side of β-sheet 1 is predominantly acidic, whereas on β-sheet 2 there is a greater balance of acidic and basic residues (Fig. 6*c*). It is worth mentioning that the HID domain is larger than the predicted DUF1533 domain, wherein β1, β2, and the loop connecting it to α1 as well as β9 are all located outside of the predicated DUF1533 domain in the primary sequence.

The HID is a structurally unique bacterial Hb-binding domain. Many species of Gram-positive bacteria that are related to *S. pyogenes* employ NEAT domains to bind Hb. Based on a Dali analysis, the Shr$^{\Delta HID2}$ and NEAT domains adopt distinct structures; their Z-score does not exceed the threshold for a strong match as defined by Holm *et al.* (60). Moreover, Shr$^{\Delta HID2}$ and NEAT domains have distinct secondary structure topologies, and Shr$^{\Delta HID2}$ lacks the conserved aromatic motif that is present in Hb-binding NEAT domains (Fig. 7, *a* and *b*). Shr$^{\Delta HID2}$ is also structurally distinct from Hb receptors found in other human pathogens, such as HpuA (61), ShuA (62), and HpHbR (63). The closest HID structural homolog in the Protein Data Bank is the CBM46 domain present in the Cel5B cellulase from *Bacillus halodurans* (PDB code 4uz8); the proteins can be superimposed with an r.m.s.d. of 2.1 Å and have a Dali Z-score of 7.9, which is deemed significant (60). However, the proteins have distinct functions, as key residues in CBM46 that mediate carbohydrate binding are poorly conserved in Shr$^{\Delta HID2}$.

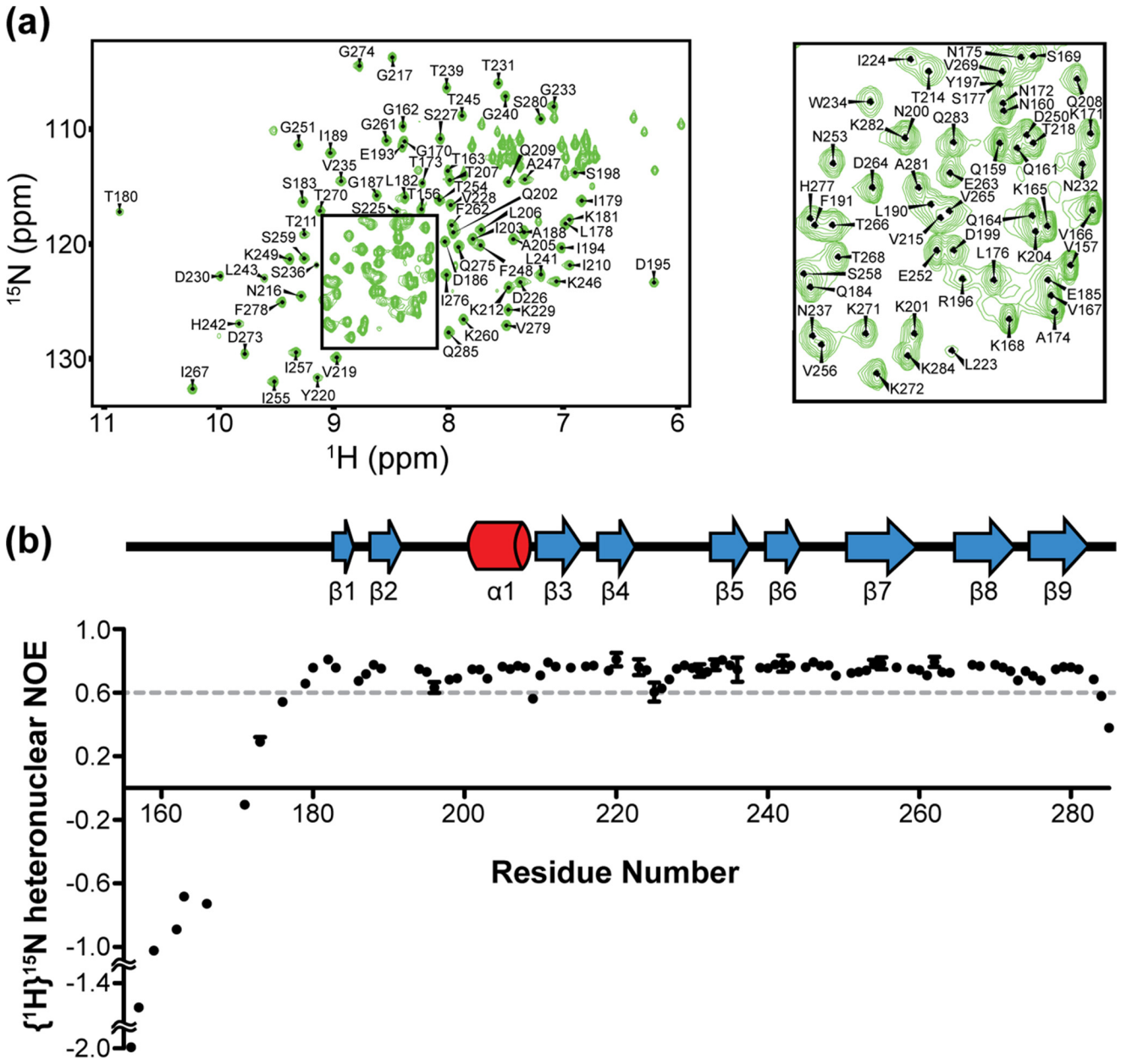

Figure 5. Assignments and dynamics data on Shr^{HID2}. *a*, backbone assignments of Shr^{HID2} overlaid onto the ^{1}H–^{15}N HSQC spectrum. *Left*, entire HSQC spectrum is shown. *Right*, *inset* shows an enlarged view of the center, which has the greatest amount of spectral overlap. Of the Shr^{HID2} construct, ~94% of the residues were assigned. Unassigned residues correspond to two prolines, two residues at the N terminus, and five residues scattered throughout the domain. *b*, {^{1}H} ^{15}N heteronuclear NOE values (on the *y* axis) shown on a per residue basis (on the *x* axis). Residues with missing heteronuclear NOE values were eliminated from the analysis due to either missing backbone assignments or severe spectral overlap. Shown are the average and standard deviation of three replicates.

HIDs within Shr^{HID1} and Shr^{HID2} engage Hb using a conserved tyrosine residue

We attempted to identify surface residues in the HID that mediate Hb binding by aligning the primary sequences of the DUF1533 domains and their flanking regions from putative Hb receptors. The primary sequences of DUF1533 domains from four Shr orthologues present in *Clostridium novyi*, *Streptococcus iniae*, *Streptococcus equi*, and *Streptococcus dysgalactiae* were aligned to Shr^{HID1} and Shr^{HID2} (Fig. S2). Six residues are universally conserved, of which only one has a side chain that is completely surface-exposed, Tyr-197 (Shr^{HID2} labeling). A Y197A mutation was introduced into Shr^{HID2} (Shr$^{HID2\text{-}Y197A}$), and its ability to bind Hb was determined using the aforementioned NMR titration experiment. In marked contrast to WT Shr^{HID2}, adding Hb to [^{15}N]Shr$^{HID2\text{-}Y197A}$ does not cause its NMR signals to broaden significantly, even when Hb is in excess (2:1 Hb/Shr$^{HID2\text{-}Y197A}$) (Fig. 8*a*). As the Y197A mutation does not disrupt the structure of Shr$^{HID2\text{-}Y197A}$, the side chain of Tyr-197 presumably forms contacts with Hb that are required for binding. The corresponding tyrosine mutation was also introduced into Shr^{HID1} (Y55A, Shr$^{HID1\text{-}Y55A}$) and was also shown to disrupt Hb binding (Fig. 8*b*). We conclude that a conserved tyrosine residue in Shr^{HID1} and Shr^{HID2} is critical for Hb binding and that the domains likely engage Hb in a similar manner.

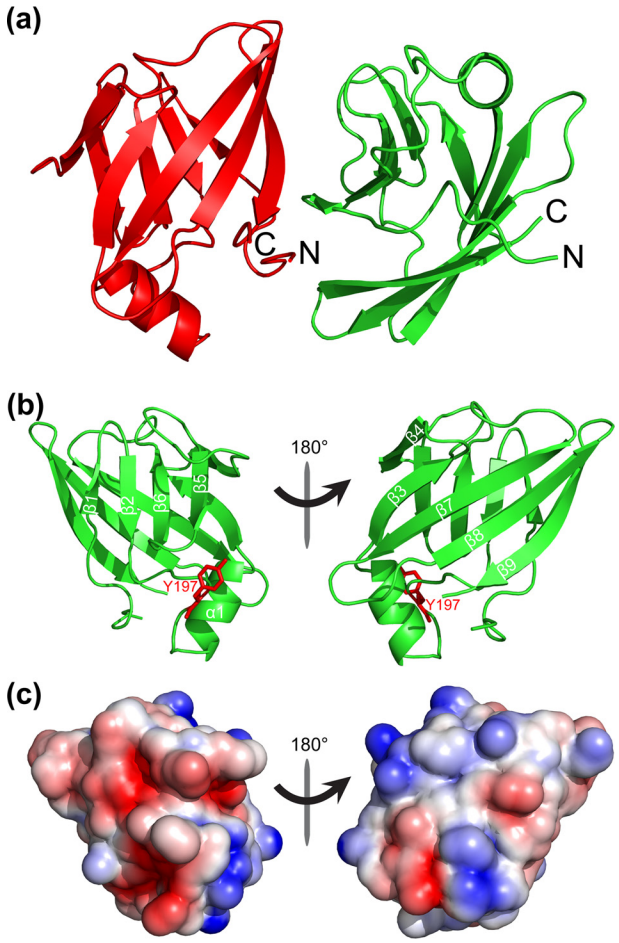

Figure 6. Crystal structure of Shr$^{\Delta HID2}$. *a*, *cartoon* representation of the two Shr$^{\Delta HID2}$ molecules in the asymmetric unit. *b*, chain B of the crystal structure with secondary structure elements labeled, and shown in *red* is the conserved tyrosine critical for Hb binding. *c*, electrostatic potential calculated using PyMOL, and shown is the same face of the domain as in *b*. *Areas shaded* in *red* and *blue* correspond to negative and positive potentials, respectively.

Table 2
Structure statistics on Shr$^{\Delta HID2}$

	Native	KI soak (SAD)
Data collection		
Beamline	APS	UCLA-HTC
Wavelength (Å)	0.9793	1.5418
Space group	$P2_12_12_1$	$P2_12_12_1$
Cell dimensions		
a, *b*, and *c* (Å)	32.47, 59.14, 102.71	31.51, 57.90, 102.00
α, β, γ (°)	90, 90, 90	90, 90, 90
Resolution (Å)	19.4–1.5 (1.554–1.5)[a]	19.4–1.818 (1.883–1.818)
R_{merge}	0.04259 (0.5419)	0.0295 (0.08212)
R_{meas}	0.04649 (0.5921)	0.03443 (0.1068)
R_{pim}	0.01836 (0.2356)	0.01761 (0.06735)
Mean $I/\sigma(I)$	23.21 (3.34)	28.78 (8.12)
Completeness (%)	99.75 (99.63)	99.66 (99.61)
No. of total reflections	206,028 (19825)	114,307 (3963)
No. of unique reflections	32,457 (3194)	32,554 (1808)
Multiplicity	6.3 (6.2)	3.5 (2.0)
Wilson *B*-factor	19.84	18.98
$CC_{1/2}$	0.999 (0.914)	0.999 (0.985)
CC^*	1 (0.977)	1 (0.996)
Refinement		
Resolution (Å)	19.7–1.5 (1.55–1.5)	
No. of reflections	32,457	
R_{work}/R_{free}	0.197/0.222 (0.2388/0.2685)	
No. of atoms	1824	
Protein	1696	
Sulfate	15	
Water	113	
Average *B*-factors		
Protein	25.22	
Sulfate	54.15	
Water	29.91	
r.m.s.d.		
Bond lengths (Å)	0.010	
Bond angles (°)	1.17	
Ramachandran plot		
Favored (%)	95.35	
Allowed (%)	4.65	
Outliers (%)	0.00	
PDB code	6DKQ	

[a] Statistics for the highest resolution shell are shown in parentheses.

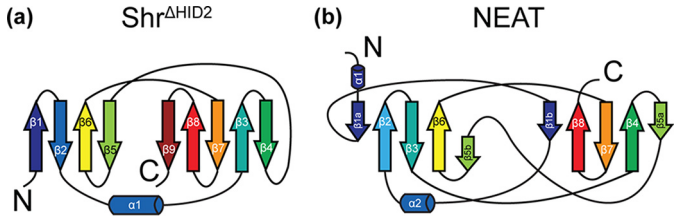

Figure 7. Domain topology of Shr$^{\Delta HID2}$ *versus* NEAT domains. *a* and *b*, secondary structural elements of Shr$^{\Delta HID2}$ showing the domain topology (*a*) compared with that of the canonical Hb-binding NEAT domains from *S. aureus* (*b*). Both domains are colored *purple* to *red* from the N to C terminus, respectively.

Discussion

Human hemoglobin is a rich source of iron that bacterial pathogens capture using surface-displayed and secreted Hb receptors (64). In Gram-positive bacteria, these receptors typically interact with Hb via NEAT domains (23). Interestingly, the Hb receptor in *S. pyogenes*, called Shr, appears to bind Hb via a novel mechanism. Its primary sequence has been divided into two regions: NTR that binds Hb, and CTR that binds hemin (8, 11). Intriguingly, based on its primary sequence, the NTR does not contain a NEAT domain suggesting that it engages Hb in a unique manner. To learn how Shr interacts with Hb, we first used NMR spectroscopy to delineate residues within its NTR that form autonomously folded domains. Three regions within the NTR are structured, two modules previously defined as domains of unknown function (DUF1533 domains) and a third module located near the C terminus of the NTR that is predicted to contain several α-helices (Fig. 1). NMR titration experiments conclusively demonstrate that only the DUF1533 domains within the NTR interact with Hb (Fig. 2). They therefore represent previously uncharacterized HIDs. In Shr they are HID1 (residues 26–148) and HID2 (residues 155–285). Interactions originating from HID2 contribute significantly to Shr's Hb binding affinity, because based on ITC measurements it binds to Hb with a $K_D = 16.0 \pm 3.4$ μM, whereas the isolated HID1 domain has significantly weaker affinity ($K_D = \sim 140$ μM). Studies of a polypeptide containing both domains (Shr^{HID1-2}), suggest avid binding to Hb. The 3-fold decrease in K_D (5.1 ± 0.4 μM) afforded by HID1 in the Shr^{HID1-2} construct would seem to indicate that binding of one HID domain facilitates binding of the other resulting in the higher apparent affinity observed for the Shr^{HID1-2}–Hb interaction. Tsumoto and co-workers (11) have measured the binding affinity of residues Gln-22–Val-364 of Shr, which contains both HIDs and the linker domain within the NTR. This polypeptide binds to Hb with similar affinity as Shr^{HID1-2} ($K_D = 6.7$ μM), further demonstrating that only the HIDs within the NTR mediate Hb binding.

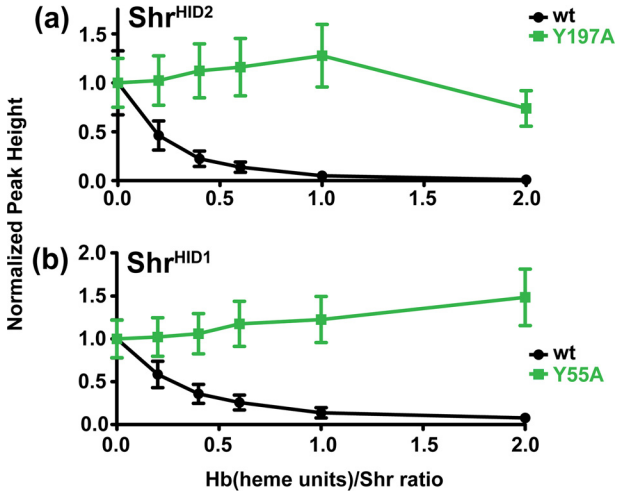

Figure 8. Hb titration experiments with Shr^{HID1} and Shr^{HID2} mutants by NMR. *a* and *b*, normalized height of peaks in the ^{1}H–^{15}N HSQC spectra (*y* axis) of [^{15}N]Shr^{HID2} and [^{15}N]Shr^{HID1} WT (*black*) as well as [^{15}N]Shr$^{HID2\text{-}Y197A}$ and [^{15}N]Shr$^{HID1\text{-}Y55A}$ (*green*) upon titrating the sample with Hb (*x* axis). Individual data points represent the average height of peaks used in the analysis, and *error bars* represent the standard deviation of those peaks used to calculate the average. Data points were normalized to the corresponding ^{1}H–^{15}N HSQC spectrum prior to adding Hb.

The crystal structure of HID2 reveals that it adopts a compact β-sandwich type fold that is distinct from previously characterized Hb-binding proteins (Fig. 6*b*). Structures of three different NEAT domains in complex with Hb have been determined, including the first and second NEAT domains from the *S. aureus* IsdH receptor (IsdH^{N1} and IsdH^{N2}) and the first NEAT domain from the *S. aureus* IsdB protein (IsdB^{N1}) (44, 50, 65). These NEAT domains share significant primary sequence homology with one another and engage Hb in a similar manner. The globin chain in Hb is contacted by residues in the NEAT domains that are located in an α-helix that is positioned between strands β1b and β2, and by residues located within nearby loops (loops connecting strands β3–β4 and β5b–β6). Each NEAT domain contains a conserved aromatic signature sequence ((F/Y)YH(F/Y)) that forms the Hb contacting α-helix that when mutated disrupts binding. The HIDs within Shr must bind to Hb in a fundamentally distinct manner, as their tertiary structures differ substantially from NEAT domains. Moreover, HID primary sequences do not contain the Hb-contacting aromatic motif. Atomic structures of other Hb receptors from eukaryotic and Gram-negative microbes have also been determined and do not share significant structural homology with the HID.

To identify the surface on HIDs that contact Hb, we compared their primary sequences and performed targeted mutagenesis. Six residues are completely conserved, but only Tyr-197 (HID2 numbering) is fully solvent-exposed in the structure of HID2 and conserved. Tyr-197 is located in the extended loop that precedes the α-helix and is surrounded by other less well-conserved residues that may mediate Hb interactions. Mutational exchange of the tyrosine to alanine in either HID1 or HID2 abrogates Hb binding, substantiating its functional importance (Fig. 8). The HID was originally named DUF1533. At present, more than 150 proteins containing DUF1533 domains from 71 distinct species of bacteria are known. Notably, these conserved tyrosine residues lie outside the predicted DUF1533 domains in the N-terminal regions of the HIDs. It is therefore unclear whether all of these sequence-related domains will also bind Hb, as some lack the key tyrosine residue and they are present in proteins that are unlikely to be orthologs of Shr because they contain other domains that are predicted to have enzymatic functions.

In vitro binding studies indicate that a single Hb tetramer is engaged by two Shr receptors. SEC-MALS experiments demonstrate that a Shr^{HID1-2} polypeptide containing both HID1 and HID2 forms a complex with the Hb tetramer that has 2:1 stoichiometry (Fig. 3*e*). It is likely that the intact Shr protein binds with similar stoichiometry, as residues outside the NTR do not mediate interactions with Hb (8). Within the 2:1 Shr^{HID1-2}–Hb complex, we speculate that HID1 and HID2 domains likely engage distinct sites on the Hb tetramer. In this scenario, each of the domains would bind a globin subunit, with interactions originating from HID2 being the most important. This model is supported by the stoichiometry obtained for the Shr^{HID1-2}–Hb interaction by SEC-MALS. It is also consistent with the results of the NMR experiments that showed that the isolated domains competitively bind Hb if it is assumed that the high-protein concentrations used in the NMR studies caused the domains to promiscuously bind to the globin subunits and/or the domains bind differently to Hb in isolation as compared with Shr^{HID1-2}. Furthermore, the mutagenesis studies in combination with the NMR competition experiments suggest that both HID's engage Hb via the same interface. Taken together, this leads us to conclude that each globin chain likely contains a single HID-binding site. It is interesting to note that HID binding to Hb is entropically unfavorable for both the isolated domains and Shr^{HID1-2} (Table 1). It is possible that residues within the domain(s) undergo a disorder to order transition upon binding Hb, as is the case for the Hb-binding NEAT domains within the IsdH and IsdB *S. aureus* Hb receptors (50, 65). However, the origin of this effect remains unclear, as the heteronuclear NOE data of apo-HID2 do not reveal the presence of large disordered loops. Structures of the Shr–:Hb complex are required to understand the molecular origins of these energetic effects.

Based on the domain architecture that we have elucidated, Shr may use a tri-domain unit to extract hemin from Hb. Only the heme extraction mechanisms used by the *S. aureus* IsdB and IsdH proteins are well-understood. These proteins share similar primary sequences and extract hemin from Hb using a tri-domain unit, in which a helical domain separates N- and C-terminal NEAT domains that bind to Hb and hemin, respectively (42). Detailed studies of IsdH indicate that its N-terminal NEAT domain (N2 domain) engages the A-helix within a globin chain contributing ~95% of the total binding standard free energy (43). This positions the remaining helical and NEAT domains near the hemin pocket on the same globin subunit, thereby enabling them to distort Hb's F-helix to trigger hemin release. IsdB also contains a homologous tri-domain unit that binds to Hb in a similar manner (50). Interestingly, Shr contains a hemin- binding NEAT domain (NEAT1) immediately following the HID2 and linker domains we have identified (Fig. 1). Thus, residues 175–502 in Shr form a

D2–linker–NEAT1 tri-domain segment that is similar to those present in IsdB and IsdH. It is possible that Shr uses a similar mechanism as IsdH/B to accelerate hemin release from Hb in which HID2 binds to a globin chain to "deliver" the NEAT1 domain near Hb's hemin pocket. Interestingly, both the Shr and IsdH receptors supplement their tri-domain segments with an additional N-terminal Hb-binding domain (HID1 in Shr and the N1 NEAT domain in IsdH). Recent studies indicate that the supplemental N1 domain in IsdH may function to slow the rate of Hb removal from the blood by obstructing interactions with the macrophage-specific endocytic receptor CD163, thereby advantageously prolonging microbial access to Hb's heme iron (66). Additional studies will be needed to determine whether the HID1 domain in Shr performs a similar function.

Collectively, the data presented in this paper provide new insight into how Shr captures Hb on the cell surface. *S. pyogenes* presumably encounters the dimeric form of Hb, as rupture of the red blood cells is expected to dramatically dilute Hb causing the tetramer to dissociate in $\alpha\beta$ dimers. As we have shown that two receptors bind a Hb tetramer, on the cell surface Shr likely engages the Hb $\alpha\beta$ dimer with 1:1 stoichiometry, such that its HID1 and HID2 domains each engage a globin subunit. Based on previous hemin transfer studies between Shr and Hb (8, 9), it seems likely that Hb's hemin molecule is transferred to Shr's NEAT1 domain, which is proximally positioned to HID2. The domain architecture of $Shr^{HID2–L–N1}$ is similar to $IsdH^{N2N3}$, a Hb- and a hemin-binding domain separated by an α-helical linker. We have previously shown that $IsdH^{N2N3}$ accelerates hemin release from Hb by interactions with the linker domain, which distorts the Hb's F-helix (45, 46). The similar domain architecture between $IsdH^{N2N3}$ and Shr suggests that the linker domain in Shr may also facilitate hemin release after it engages Hb. Further insight into the mechanism of Hb capture will be gained by structural studies on the Shr–Hb complex.

Experimental procedures

Cloning, protein expression, and purification

Standard methods were used to construct expression plasmids that produced the following polypeptides: Shr^{HID1} (residues 26–148); Shr^{HID2} (residues 155–285); $Shr^{\Delta HID2}$ (residues 175–285); $Shr^{HID1–2}$ (residues 26–285); and Shr^{L} (residues 294–364). Proteins were expressed from pSUMO-based vectors (LifeSensors) that were transformed into *Escherichia coli* BL21(DE3) cells (New England Biolabs, Beverly, MA). Cultures were grown at 37 °C to an A_{600} of 0.6–0.8 before induction with isopropyl β-D-thiogalactoside at a final concentration of 1 mM. Induction proceeded at 25 °C overnight before harvesting the cells by centrifugation. The cell pellet was then resuspended in lysis buffer containing: 50 mM NaH_2PO_4/Na_2HPO_4, pH 7.0, 300 mM NaCl. A protease inhibitor mixture (Calbiochem) and phenylmethylsulfonyl fluoride (Sigma) was also added to the lysis buffer. Cells were lysed by sonication, and the lysate was clarified by centrifugation (27,200 × *g*). The lysate was then loaded onto a Co^{2+}-chelating column (ThermoFisher Scientific, Waltham, MA), and unbound proteins were removed by washing the column with lysis buffer (5 column volume (CV) equivalents). Nonspecifically bound proteins were also removed by applying 5 CVs of wash buffer (lysis buffer + 10 mM imidazole) and 5 CVs of lysis buffer. The N-terminal His_6–SUMO tag was then cleaved with the ULP1 protease and eluted by washing the column with lysis buffer. If necessary, proteins were purified using an SEC column as described by the vendor (Sephacryl, GE Healthcare). Human Hb was prepared as described previously from the blood of a healthy donor provided by the CFAR Virology Core Lab at the UCLA AIDS Institute (43). Purified Hb0.1 was a generous gift of the Olson laboratory.

NMR spectroscopy

Uniformly ^{13}C- and ^{15}N-labeled Shr^{HID2} was expressed in *E. coli* BL21(DE3) cells grown in M9 medium supplemented with $^{15}NH_4Cl$ and [$^{13}C_6$]glucose. The NMR sample of Shr^{HID2} contained 1.1 mM [U-^{15}N,U-^{13}C]Shr(155–285) dissolved in 50 mM NaH_2PO_4/Na_2HPO_4, pH 6.0, 50 mM NaCl, 0.01% NaN_3 with 92:8% H_2O/D_2O. NMR experiments were performed at 298 K on Bruker DRX 500, DRX 600 MHz, and AVANCE 800 MHz spectrometers equipped with triple resonance cryogenic probes. NMR spectra were processed using NMRPipe (67) and TopSpin3 (68) and analyzed using CARA (69). Backbone ^{1}H, ^{13}C, and ^{15}N chemical shifts were assigned by analyzing data from the following experiments: 2D ^{1}H-^{15}N HSQC, 2D ^{1}H-^{13}C HSQC, 3D CBCA(CO)NH, HNCACB, HNCO, HN(CA)CO, HNCA, HNHA, HNHB, HBHA(CO)NH, HBHANH, and CC(CO)NH (Fig. 5*a*). Assignments have been deposited to the BMRB under accession number 27550. Heteronuclear {^{1}H} ^{15}N NOE experiments were collected in an interleaved manner and analyzed using Sparky (70). The average and standard deviation of three replicates are reported (Fig. 5*b*).

NMR Hb titration experiments employed 200 μM uniformly ^{15}N-labeled Shr constructs that were dissolved in 50 mM NaH_2PO_4/Na_2HPO_4, pH 6.8, 100 mM NaCl, 92% H_2O/8% D_2O. The Hb titrant was dissolved in 50 mM NaH_2PO_4/Na_2HPO_4, pH 6.8, 100 mM NaCl and added from a 3.5–5.5 mM stock solution (heme units). Hb was added to the sample at a 1:1 ratio of tetramer to ^{15}N-labeled Shr construct. The NMR competition experiments were carried using conditions that were similar to those used for the Hb titration experiments. A sample of uniformly ^{15}N-labeled Shr^{HID1} dissolved in 50 mM NaH_2PO_4/Na_2HPO_4, pH 6.8, 100 mM NaCl, 92% H_2O/8% D_2O to a final concentration of 200 μM was prepared. Buffer-matched Hb in its carbonmonoxy state was then added such that the final ratio was 1:2, [^{15}N]Shr^{HID1}/Hb. Unlabeled Shr^{HID2} was then added to achieve a ratio of [^{15}N]Shr^{HID1}/Hb/Shr^{HID2} = 1:2:2 or 1:2:4. All samples were incubated for 30 min at room temperature prior to data acquisition. For each ^{1}H–^{15}N HSQC experiment, the number of scans was adjusted to compensate for changes in protein concentration.

Isothermal titration calorimetry (ITC)

ITC measurements were performed using a MicroCal iTC200 calorimeter (GE Healthcare) at 25 °C. The Hb (in the

carbonmonoxy state) and Shr constructs were buffer-matched in 20 mM NaH_2PO/Na_2HPO_4, pH 7.5, 150 mM NaCl, 450 mM sucrose. The cell was filled with 25–35 μM Hb (concentration reported on a heme/globin chain basis), and the syringe was filled with either 700 μM Shr^{HID1}, 500 μM Shr^{HID2}, 550–600 μM $Shr^{\Delta HID2}$, or 350–500 μM Shr^{HID1-2}. Twenty injections were performed using 2.0-μl injection volumes at 180-s intervals. For each of the Shr constructs, an experiment was carried out to control for the heats of dilution in which the respective Shr construct was titrated into buffer, and the control data were subtracted from the experimental data. ORIGIN software was used to fit the data to a single-site binding model.

SEC-MALS

The analytical size-exclusion column WTC-030S5 (Wyatt Technology) was equilibrated in 20 mM NaH_2PO/Na_2HPO_4, pH 7.5, 150 mM NaCl using an AKTA pure (GE Healthcare). For each protein or complex, a 100-μl (buffer-matched) sample was loaded: 1.2 mM HbCO (heme basis), 600 μM Shr^{HID1-2}, and the complex of HbCO at 1.2 mM and Shr^{HID1-2} at 600 μM, 1.2 mM, and 1.8 mM. During elution, light scattering was measured with a miniDAWN TREOS (Wyatt Technology), and the refractive index (n) was measured with an Optilab T-rEX system (Wyatt Technology). Data were analyzed using ASTRA software (version 6.1) to obtain average molecular weights. The dn/dc value (where c is the concentration) for the calculation was set to 0.185 ml/g for Hb (66). Based on the primary sequence, the dn/dc values for Shr^{HID1-2} and $Shr^{\Delta HID2}$ were calculated to be 0.187 and 0.188 ml/g, respectively. For the complex of Shr^{HID1-2} with Hb, the dn/dc value was calculated to be 0.186 ml/g based on the equation for the weight average sum. Theoretical molecular weights were obtained using the ProtParam server based on the primary amino acid sequence (58).

Analytical ultracentrifugation (AUC)

Sedimentation equilibrium experiments were performed at 20 °C using a Beckman Optima XL-A analytical ultracentrifuge equipped with an An60-Ti rotor. Native HbA has a dimer/tetramer equilibrium, which complicates the determination of the Shr^{HID2}–Hb binding stoichiometry by AUC. To simplify the analysis, a mutant variety of Hb, which stabilizes the tetrameric form, was employed (Hb0.1) (71, 72). Absorption optics at 280 nm were carried out for Shr^{HID2} alone and at 412 nm for Hb0.1 alone or in complex with Shr^{HID2} so that only the heme molecule was detected. All experiments were carried out in 20 mM NaH_2PO/Na_2HPO_4, pH 7.5, 150 mM NaCl. 450 mM sucrose. To prevent heme release, Hb0.1 in the carbon monoxide state was used. Three mm pathlength double sector cells were used for all samples and were purged with CO before sealing the cells to prevent oxidation. Sedimentation equilibrium profiles were measured at 8,000 (~5,200 × g), 11,000 (~9,700 × g), and 26,000 rpm (~54,500 × g) for Shr^{HID2} alone, with the last being used for the analysis. For Hb0.1 alone and in complex with Shr^{HID2}, sedimentation equilibrium profiles were measured at 11,000 (~9,700 × g) and 13,000 rpm (~13,600 × g), with the latter being used for the analysis. A third measurement was made at 30,000 rpm (~72,500 × g) and was used to determine the baseline. Samples of Hb0.1 and Shr^{HID2} alone contained 5.5 and 248 μM protein, respectively. For data collected at a 15:1 ratio of Shr^{D2}/Hb0.1, the sample contained 6.2 and 89 μM Hb0.1 and Shr^{HID2}, respectively. For the 45:1 ratio of Shr^{HID2}/Hb0.1, the sample contained 5.5 and 248 μM Hb0.1 and Shr^{HID2}, respectively. Weight average molecular masses were determined by fitting with a nonlinear least-squares exponential fit for a single ideal species using Beckman Origin-based software (version 3.01). Partial specific volumes were calculated from the amino acid compositions and corrected to 20 °C. They were 0.740 for Shr^{HID2}, 0.749 for Hb0.1, and 0.746 for the complex.

X-ray crystallography

Crystals of $Shr^{\Delta HID2}$ were produced from a stock of 52 mg/ml (4.2 mM) dissolved in 20 mM NaH_2PO_4/Na_2HPO_4, pH 6.5. Crystals were grown using the hanging drop, vapor diffusion method against a mother liquor of 0.1 M sodium acetate, pH 4.5, 0.1–0.2 M lithium sulfate, 30–50% (w/v) PEG 400. Crystals developed after ~24 h at room temperature. Data sets were collected on two crystals: $Shr^{\Delta HID2}$ (native) and $Shr^{\Delta HID2}$ soaked for 30 s in mother liquor containing 35.9% (w/v) PEG 400 and 460 mM KI ($Shr^{\Delta HID2}$ + KI) (73). The KI dataset was collected on a Rigaku FRE+ generator with a copper anode equipped with a Rigaku HTC image plate detector (λ = 1.5418 Å). The Matthews coefficient indicated that there were two $Shr^{\Delta HID2}$ molecules in the asymmetric unit using the online server MATTPROB (74). XDS/XSCALE was used to index, integrate, and scale the data (75). Conservative resolution limits were applied to balance the calculated I/σ, R_{sym}, and $CC1/2$ in the highest resolution shell. The structure of $Shr^{\Delta HID2}$ was solved by single-wavelength anomalous dispersion on $Shr^{\Delta HID2}$ + KI using HKL2MAP (76), the graphical user interface for the SHELXC/D/E programs. Four iodide sites were found by SHELXD (77). SHELXE (78) was used to assign the hand, produce the first set of phases, and perform solvent flattening. The final figure of merit was 0.767. Further density modification and automatic model building was performed by SHARP (79). SHARP built residues 2–111 of chain A and 8–109 of chain B in the initial model out of 112 residues in the construct. The $Shr^{\Delta HID2}$ + KI model was refined to 1.8 Å. This model was further refined against the high-resolution 1.5 Å native data set obtained at the Advanced Photon Source on beamline 24-ID-C on a DECTRIS-PILATUS 6M detector (λ = 0.9793 Å). Initial rounds of structure refinement were carried out using Coot (80) and PHENIX (81). Later rounds of refinement were carried out using Coot (80) and BUSTER (82) with TLS refinement (83). Structure statistics are presented in Table 2. The coordinates of the final model and structure factors have been deposited in the Protein Data Bank under PDB code 6DKQ.

Author contributions—R. M. and R. T. C. conceptualization; R. M., D. C., and M. L. P. data curation; R. M., D. C., and M. L. P. formal analysis; R. M. investigation; R. M. and R. T. C. writing-original draft; D. C., M. J. C., and M. L. P. resources; D. C. and M. L. P. software; D. C. and M. L. P. validation; D. C. methodology; R. T. C. supervision; R. T. C. funding acquisition; R. T. C. project administration.

Acknowledgments—We thank Dr. Robert Peterson for assistance with NMR experiments. We also thank Dr. Brendan R. Amer and Orlando Martinez for assistance with the SEC-MALS experiments and Dr. William Silkworth for assistance with ITC experiments. We are grateful for useful discussions with Dr. Megan Sjodt, as well as members of the Clubb laboratory. We thank Professors Zehava Eichenbaum and John Olson for providing useful reagents. NMR equipment used in this research was purchased using funds from shared National Institutes of Health Equipment Grant S10OD016336. This work is based upon research conducted at the Northeastern Collaborative Access Team beamlines that are funded by National Institutes of Health Grant P41 GM103403 from NIGMS. The Pilatus 6M detector on 24-ID-C beam line is funded by National Institutes of Health-ORIP HEI Grant S10 RR029205. This research used resources of the Advanced Photon Source, a United States Department of Energy (DOE) Office of Science User Facility operated for the DOE Office of Science by Argonne National Laboratory under Contract No. DE-AC02–06CH11357.

References

1. Zhu, L., Charbonneau, A. R. L., Waller, A. S., Olsen, R. J., Beres, S. B., and Musser, J. M. (2017) Novel genes required for the fitness of *Streptococcus pyogenes* in human saliva. *mSphere* **2,** e00460-17 Medline
2. Carapetis, J. R., Steer, A. C., Mulholland, E. K., and Weber, M. (2005) The global burden of group A streptococcal diseases. *Lancet Infect. Dis.* **5,** 685–694 Medline
3. Stevens, D. L. (1995) Streptococcal toxic-shock syndrome: spectrum of disease, pathogenesis, and new concepts in treatment. *Emerg. Infect. Dis.* **1,** 69–78 CrossRef Medline
4. Tsatsaronis, J. A., Walker, M. J., and Sanderson-Smith, M. L. (2014) Host responses to group A *Streptococcus*: cell death and inflammation. *PLoS Pathog.* **10,** e1004266 Medline
5. Ralph, A. P., and Carapetis, J. R. (2013) Group A streptococcal diseases and their global burden. *Curr. Top. Microbiol. Immunol.* **368,** 1–27 Medline
6. Ge, R., and Sun, X. (2014) Iron acquisition and regulation systems in *Streptococcus* species. *Metallomics* **6,** 996–1003 CrossRef Medline
7. Bates, C. S., Montañez, G. E., Woods, C. R., Vincent, R. M., and Eichenbaum, Z. (2003) Identification and characterization of a *Streptococcus pyogenes* operon involved in binding of hemoproteins and acquisition of iron. *Infect. Immun.* **71,** 1042–1055 CrossRef Medline
8. Ouattara, M., Cunha, E. B., Li, X., Huang, Y. S., Dixon, D., and Eichenbaum, Z. (2010) Shr of group A *Streptococcus* is a new type of composite NEAT protein involved in sequestering haem from methaemoglobin. *Mol. Microbiol.* **78,** 739–756 CrossRef Medline
9. Lu, C., Xie, G., Liu, M., Zhu, H., and Lei, B. (2012) Direct heme transfer reactions in the group A *Streptococcus* heme acquisition pathway. *PLoS ONE* **7,** e37556 CrossRef Medline
10. Fisher, M., Huang, Y. S., Li, X., McIver, K. S., Toukoki, C., and Eichenbaum, Z. (2008) Shr is a broad-spectrum surface receptor that contributes to adherence and virulence in group A *Streptococcus*. *Infect. Immun.* **76,** 5006–5015 CrossRef Medline
11. Hoshino, M., Nakakido, M., Nagatoishi, S., Aikawa, C., Nakagawa, I., and Tsumoto, K. (2017) Biophysical characterization of the interaction between heme and proteins responsible for heme transfer in *Streptococcus pyogenes*. *Biochem. Biophys. Res. Commun.* **493,** 1109–1114 CrossRef Medline
12. Dahesh, S., Nizet, V., and Cole, J. N. (2012) Study of streptococcal hemoprotein receptor (Shr) in iron acquisition and virulence of M1T1 group A *Streptococcus*. *Virulence* **3,** 566–575 CrossRef Medline
13. Aranda, R., 4th, Worley, C. E., Liu, M., Bitto, E., Cates, M. S., Olson, J. S., Lei, B., and Phillips, G. N., Jr. (2007) Bis-methionyl coordination in the crystal structure of the heme-binding domain of the streptococcal cell surface protein Shp. *J. Mol. Biol.* **374,** 374–383 CrossRef Medline
14. Lei, B., Smoot, L. M., Menning, H. M., Voyich, J. M., Kala, S. V., Deleo, F. R., Reid, S. D., and Musser, J. M. (2002) Identification and characterization of a novel heme-associated cell surface protein made by *Streptococcus pyogenes*. *Infect. Immun.* **70,** 4494–4500 CrossRef Medline
15. Vicente, J. J., Galardi-Castilla, M., Escalante, R., and Sastre, L. (2008) The surface protein Shr of *Streptococcus pyogenes* binds heme and transfers it to the streptococcal heme-binding protein Shp. *BMC Microbiol.* **8,** 15 CrossRef Medline
16. Liu, M., and Lei, B. (2005) Heme transfer from streptococcal cell surface protein Shp to HtsA of transporter HtsABC. *Infect. Immun.* **73,** 5086–5092 CrossRef Medline
17. Ran, Y., Malmirchegini, G. R., Clubb, R. T., and Lei, B. (2013) Axial ligand replacement mechanism in heme transfer from streptococcal heme-binding protein shp to HtsA of the HtsABC transporter. *Biochemistry* **52,** 6537–6547 CrossRef Medline
18. Nygaard, T. K., Blouin, G. C., Liu, M., Fukumura, M., Olson, J. S., Fabian, M., Dooley, D. M., and Lei, B. (2006) The mechanism of direct heme transfer from the streptococcal cell surface protein Shp to HtsA of the HtsABC transporter. *J. Biol. Chem.* **281,** 20761–20771 CrossRef Medline
19. Ran, Y., Zhu, H., Liu, M., Fabian, M., Olson, J. S., Aranda, R., 4th, Phillips, G. N., Jr., Dooley, D. M., and Lei, B. (2007) Bis-methionine ligation to heme iron in the streptococcal cell surface protein Shp facilitates rapid hemin transfer to HtsA of the HtsABC transporter. *J. Biol. Chem.* **282,** 31380–31388 CrossRef Medline
20. Lei, B. (2010) Benfang Lei's research on heme acquisition in Gram-positive pathogens and bacterial pathogenesis. *World J. Biol. Chem.* **1,** 286–290 CrossRef Medline
21. Ran, Y., Liu, M., Zhu, H., Nygaard, T. K., Brown, D. E., Fabian, M., Dooley, D. M., and Lei, B. (2010) Spectroscopic identification of heme axial ligands in HtsA that are involved in heme acquisition by *Streptococcus pyogenes*. *Biochemistry* **49,** 2834–2842 CrossRef Medline
22. Andrade, M., Ciccarelli, F. D., Perez-Iratxeta, C., and Bork, P. (2002) NEAT: a domain duplicated in genes near the components of a putative Fe^{3+} siderophore transporter from Gram-positive pathogenic bacteria. *Genome Biol.* **3,** RESEARCH0047 Medline
23. Sheldon, J. R., and Heinrichs, D. E. (2015) Recent developments in understanding the iron acquisition strategies of Gram positive pathogens. *FEMS Microbiol. Rev.* **39,** 592–630 CrossRef Medline
24. Pilpa, R. M., Fadeev, E. A., Villareal, V. A., Wong, M. L., Phillips, M., and Clubb, R. T. (2006) Solution structure of the NEAT (NEAr Transporter) domain from IsdH/HarA: the human hemoglobin receptor in *Staphylococcus aureus*. *J. Mol. Biol.* **360,** 435–447 CrossRef Medline
25. Dryla, A., Hoffmann, B., Gelbmann, D., Giefing, C., Hanner, M., Meinke, A., Anderson, A. S., Koppensteiner, W., Konrat, R., von Gabain, A., and Nagy, E. (2007) High-affinity binding of the staphylococcal HarA protein to haptoglobin and hemoglobin involves a domain with an antiparallel eight-stranded β-barrel fold. *J. Bacteriol.* **189,** 254–264 CrossRef Medline
26. Watanabe, M., Tanaka, Y., Suenaga, A., Kuroda, M., Yao, M., Watanabe, N., Arisaka, F., Ohta, T., Tanaka, I., and Tsumoto, K. (2008) Structural basis for multimeric heme complexation through a specific protein-heme interaction: the case of the third NEAT domain of IsdH from *Staphylococcus aureus*. *J. Biol. Chem.* **283,** 28649–28659 CrossRef Medline
27. Liu, M., Tanaka, W. N., Zhu, H., Xie, G., Dooley, D. M., and Lei, B. (2008) Direct hemin transfer from IsdA to IsdC in the iron-regulated surface determinant (Isd) heme acquisition system of *Staphylococcus aureus*. *J. Biol. Chem.* **283,** 6668–6676 CrossRef Medline
28. Fabian, M., Solomaha, E., Olson, J. S., and Maresso, A. W. (2009) Heme transfer to the bacterial cell envelope occurs via a secreted hemophore in the Gram-positive pathogen *Bacillus anthracis*. *J. Biol. Chem.* **284,** 32138–32146 CrossRef Medline
29. Pilpa, R. M., Robson, S. A., Villareal, V. A., Wong, M. L., Phillips, M., and Clubb, R. T. (2009) Functionally distinct NEAT (NEAr transporter) domains within the *Staphylococcus aureus* IsdH/HarA protein extract heme from methemoglobin. *J. Biol. Chem.* **284,** 1166–1176 CrossRef Medline
30. Villareal, V. A., Spirig, T., Robson, S. A., Liu, M., Lei, B., and Clubb, R. T. (2011) Transient weak protein-protein complexes transfer heme across the cell wall of *Staphylococcus aureus*. *J. Am. Chem. Soc.* **133,** 14176–14179 CrossRef Medline

31. Gaudin, C. F. M., Grigg, J. C., Arrieta, A. L., and Murphy, M. E. (2011) Unique heme-iron coordination by the hemoglobin receptor IsdB of *Staphylococcus aureus*. *Biochemistry* **50,** 5443–5452 CrossRef Medline
32. Vu, N. T., Moriwaki, Y., Caaveiro, J. M., Terada, T., Tsutsumi, H., Hamachi, I., Shimizu, K., and Tsumoto, K. (2013) Selective binding of antimicrobial porphyrins to the heme-receptor IsdH-NEAT3 of *Staphylococcus aureus*. *Protein Sci.* **22,** 942–953 CrossRef Medline
33. Moriwaki, Y., Terada, T., Caaveiro, J. M., Takaoka, Y., Hamachi, I., Tsumoto, K., and Shimizu, K. (2013) Heme binding mechanism of structurally similar iron-regulated surface determinant near transporter domains of *Staphylococcus aureus* exhibiting different affinities for heme. *Biochemistry* **52,** 8866–8877 CrossRef Medline
34. Fonner, B. A., Tripet, B. P., Eilers, B. J., Stanisich, J., Sullivan-Springhetti, R. K., Moore, R., Liu, M., Lei, B., and Copié, V. (2014) Solution structure and molecular determinants of hemoglobin binding of the first NEAT domain of IsdB in *Staphylococcus aureus*. *Biochemistry* **53,** 3922–3933 CrossRef Medline
35. Moriwaki, Y., Terada, T., Tsumoto, K., and Shimizu, K. (2015) Rapid heme transfer reactions between NEAr transporter domains of staphylococcus aureus: a theoretical study using QM/MM and MD simulations. *PLoS ONE* **10,** e0145125 CrossRef Medline
36. Grigg, J. C., Vermeiren, C. L., Heinrichs, D. E., and Murphy, M. E. (2007) Haem recognition by a *Staphylococcus aureus* NEAT domain. *Mol. Microbiol.* **63,** 139–149 CrossRef Medline
37. Dryla, A., Gelbmann, D., von Gabain, A., and Nagy, E. (2003) Identification of a novel iron regulated staphylococcal surface protein with haptoglobin-haemoglobin binding activity. *Mol. Microbiol.* **49,** 37–53 CrossRef Medline
38. Villareal V. A., Pilpa, R. M., Robson, S. A., Fadeev, E. A., and Clubb, R. T. (2008) The IsdC protein from *Staphylococcus aureus* uses a flexible binding pocket to capture heme. *J. Biol. Chem.* **283,** 31591–31600 CrossRef Medline
39. Sharp, K. H., Schneider, S., Cockayne, A., and Paoli, M. (2007) Crystal structure of the heme-IsdC complex, the central conduit of the Isd iron/heme uptake system in *Staphylococcus aureus*. *J. Biol. Chem.* **282,** 10625–10631 CrossRef Medline
40. Pluym, M., Muryoi, N., Heinrichs, D. E., and Stillman, M. J. (2008) Heme binding in the NEAT domains of IsdA and IsdC of *Staphylococcus aureus*. *J. Inorg. Biochem.* **102,** 480–488 CrossRef Medline
41. Pishchany, G., Dickey, S. E., and Skaar, E. P. (2009) Subcellular localization of the *Staphylococcus aureus* heme iron transport components IsdA and IsdB. *Infect. Immun.* **77,** 2624–2634 CrossRef Medline
42. Spirig, T., Malmirchegini, G. R., Zhang, J., Robson, S. A., Sjodt, M., Liu, M., Krishna Kumar, K., Dickson, C. F., Gell, D. A., Lei, B., Loo, J. A., and Clubb, R. T. (2013) *Staphylococcus aureus* uses a novel multidomain receptor to break apart human hemoglobin and steal its heme. *J. Biol. Chem.* **288,** 1065–1078 CrossRef Medline
43. Sjodt, M., Macdonald, R., Marshall, J. D., Clayton, J., Olson, J. S., Phillips, M., Gell, D. A., Wereszczynski, J., and Clubb, R. T. (2018) Energetics underlying hemin extraction from human hemoglobin by *Staphylococcus aureus*. *J. Biol. Chem.* **293,** 6942–6957 CrossRef Medline
44. Dickson, C. F., Kumar, K. K., Jacques, D. A., Malmirchegini, G. R., Spirig, T., Mackay, J. P., Clubb, R. T., Guss, J. M., and Gell, D. A. (2014) Structure of the hemoglobin-IsdH complex reveals the molecular basis of iron capture by *Staphylococcus aureus*. *J. Biol. Chem.* **289,** 6728–6738 CrossRef Medline
45. Dickson, C. F., Jacques, D. A., Clubb, R. T., Guss, J. M., and Gell, D. A. (2015) The structure of haemoglobin bound to the haemoglobin receptor IsdH from *Staphylococcus aureus* shows disruption of the native α-globin haem pocket. *Acta Crystallogr. D Biol. Crystallogr.* **71,** 1295–1306 CrossRef Medline
46. Sjodt, M., Macdonald, R., Spirig, T., Chan, A. H., Dickson, C. F., Fabian, M., Olson, J. S., Gell, D. A., and Clubb, R. T. (2016) The PRE-derived NMR model of the 38.8-kDa tri-domain IsdH protein from *Staphylococcus aureus* suggests that it adaptively recognizes human hemoglobin. *J. Mol. Biol.* **428,** 1107–1129 CrossRef Medline
47. Bowden, C. F., Verstraete, M. M., Eltis, L. D., and Murphy, M. E. (2014) Hemoglobin binding and catalytic heme extraction by IsdB near iron transporter domains. *Biochemistry* **53,** 2286–2294 CrossRef Medline
48. Zhu, H., Li, D., Liu, M., Copié, V., and Lei, B. (2014) Non-heme-binding domains and segments of the *Staphylococcus aureus* IsdB protein critically contribute to the kinetics and equilibrium of heme acquisition from methemoglobin. *PLoS ONE* **9,** e100744 CrossRef Medline
49. Pishchany, G., Sheldon, J. R., Dickson, C. F., Alam, M. T., Read, T. D., Gell, D. A., Heinrichs, D. E., and Skaar, E. P. (2014) IsdB-dependent hemoglobin binding is required for acquisition of heme by *Staphylococcus aureus*. *J. Infect. Dis.* **209,** 1764–1772 CrossRef Medline
50. Bowden, C. F. M., Chan, A. C. K., Li, E. J. W., Arrieta, A. L., Eltis, L. D., and Murphy, M. E. P. (2018) Structure-function analyses reveal key features in *Staphylococcus aureus* IsdB-associated unfolding of the heme-binding pocket of human hemoglobin. *J. Biol. Chem.* **293,** 177–190 CrossRef Medline
51. Malmirchegini, G. R., Sjodt, M., Shnitkind, S., Sawaya, M. R., Rosinski, J., Newton, S. M., Klebba, P. E., and Clubb, R. T. (2014) Novel mechanism of hemin capture by Hbp2, the hemoglobin-binding hemophore from *Listeria monocytogenes*. *J. Biol. Chem.* **289,** 34886–34899 CrossRef Medline
52. Maresso, A. W., Garufi, G., and Schneewind, O. (2008) *Bacillus anthracis* secretes proteins that mediate heme acquisition from hemoglobin. *PLoS Pathog.* **4,** e1000132 CrossRef Medline
53. Honsa, E. S., Fabian, M., Cardenas, A. M., Olson, J. S., and Maresso, A. W. (2011) The five near-iron transporter (NEAT) domain anthrax hemophore, IsdX2, scavenges heme from hemoglobin and transfers heme to the surface protein IsdC. *J. Biol. Chem.* **286,** 33652–33660 CrossRef Medline
54. Balderas, M. A., Nobles, C. L., Honsa, E. S., Alicki, E. R., and Maresso, A. W. (2012) Hal is a *Bacillus anthracis* heme acquisition protein. *J. Bacteriol.* **194,** 5513–5521 CrossRef Medline
55. Ouattara, M., Pennati, A., Devlin, D. J., Huang, Y. S., Gadda, G., and Eichenbaum, Z. (2013) Kinetics of heme transfer by the Shr NEAT domains of group A *Streptococcus*. *Arch. Biochem. Biophys.* **538,** 71–79 CrossRef Medline
56. Buchan, D. W., Minneci, F., Nugent, T. C., Bryson, K., and Jones, D. T. (2013) Scalable web services for the PSIPRED protein analysis workbench. *Nucleic Acids Res.* **41,** 349–357 Medline
57. Drozdetskiy, A., Cole, C., Procter, J., and Barton, G. J. (2015) JPred4: a protein secondary structure prediction server. *Nucleic Acids Res.* **43,** W389–W394 CrossRef Medline
58. Gasteiger, E., Hoogland, C., Gattiker, A., Duvaud, S., Wilkins, M. R., Appel, R. D., and Bairoch, A. (2005) *Protein Identification and Analysis Tools on the ExPASy Server*. in *The Proteomics Protocols Handbook* (Walker, J. M., ed) pp. 571–607, Humana Press Inc., Totowa, NJ
59. DeLano, W. L. (2004) *PyMOL User's Guide,* Version 1.4, DeLano Scientific LLC, San Carlos, CA
60. Holm, L., Kääriäinen, S., Rosenström, P., and Schenkel, A. (2008) Searching protein structure databases with DaliLite v.3. *Bioinformatics* **24,** 2780–2781 CrossRef Medline
61. Wong, C. T., Xu, Y., Gupta, A., Garnett, J. A., Matthews, S. J., and Hare, S. A. (2015) Structural analysis of haemoglobin binding by HpuA from the Neisseriaceae family. *Nat. Commun.* **6,** 10172 CrossRef Medline
62. Cobessi, D., Meksem, A., and Brillet, K. (2010) Structure of the heme/hemoglobin outer membrane receptor ShuA from *Shigella dysenteriae*: heme binding by an induced fit mechanism. *Proteins* **78,** 286–294 CrossRef Medline
63. Stødkilde, K., Torvund-Jensen, M., Moestrup, S. K., and Andersen, C. B. (2014) Structural basis for trypanosomal haem acquisition and susceptibility to the host innate immune system. *Nat. Commun.* **5,** 5487 CrossRef Medline
64. Hare, S. A. (2017) Diverse structural approaches to haem appropriation by pathogenic bacteria. *Biochim. Biophys. Acta* **1865,** 422–433 CrossRef
65. Krishna Kumar, K., Jacques, D. A., Pishchany, G., Caradoc-Davies, T., Spirig, T., Malmirchegini, G. R., Langley, D. B., Dickson, C. F., Mackay, J. P., Clubb, R. T., Skaar, E. P., Guss, J. M., and Gell, D. A. (2011) Structural basis for hemoglobin capture by *Staphylococcus aureus* cell-surface protein, IsdH. *J. Biol. Chem.* **286,** 38439–38447 CrossRef Medline

66. Sæderup, K. L., Stødkilde, K., Graversen, J. H., Dickson, C. F., Etzerodt, A., Hansen, S. W., Fago, A., Gell, D., Andersen, C. B., and Moestrup, S. K. (2016) The *Staphylococcus aureus* protein IsdH inhibits host hemoglobin scavenging to promote heme acquisition by the pathogen. *J. Biol. Chem.* **291,** 23989–23998 CrossRef Medline
67. Delaglio, F., Grzesiek, S., Vuister, G. W., Zhu, G., Pfeifer, J., and Bax, A. (1995) NMRPipe: a multidimensional spectral processing system based on UNIX pipes*. *J. Biomol. NMR* **6,** 277–293 Medline
68. NMR Software Department (2016) *TopSpin: NMRData Publishing User Manual*, Bruker BioSpin GmbH, Rheinstetten, Germany
69. Keller, R. (2004) *The Computer Aided Resonance Assignment Tutorial.* 1st Ed., Cantina Verlag, Goldau, Switzerland
70. Goddard, T. D., and Kneller, D. G. (2006) *Sparky3,* University of California, San Francisco
71. Looker, D., Abbott-Brown, D., Cozart, P., Durfee, S., Hoffman, S., Mathews, A. J., Miller-Roehrich, J., Shoemaker, S., Trimble, S., and Fermi, G. (1992) A human recombinant haemoglobin designed for use as a blood substitute. *Nature* **356,** 258–260 CrossRef Medline
72. Looker, D., Mathews, A. J., Neway, J. O., and Stetler, G. L. (1994) Expression of recombinant human hemoglobin in *Escherichia coli*. *Methods Enzymol.* **231,** 364–374 CrossRef Medline
73. Dauter, Z., Dauter, M., and Rajashankar, K. R. (2000) Novel approach to phasing proteins: derivatization by short cryo-soaking with halides. *Acta Crystallogr. Sect. D Biol. Crystallogr.* **56,** 232–237 CrossRef
74. Kantardjieff, K. A., and Rupp, B. (2003) Matthews coefficient probabilities: Improved estimates for unit cell contents of proteins, DNA, and protein-nucleic acid complex crystals. *Protein Sci.* **12,** 1865–1871 CrossRef Medline
75. Kabsch, W. (2010) XDS. *Acta Crystallogr. Sect. D Biol. Crystallogr.* **66,** 125–132 CrossRef
76. Pape, T., and Schneider, T. R. (2004) HKL2MAP: a graphical user interface for macromolecular phasing with *SHELX* programs. *J. Appl. Crystallogr.* **37,** 843–844 CrossRef
77. Usón, I., and Sheldrick, G. M. (1999) Advances in direct methods for protein crystallography. *Curr. Opin. Struct. Biol.* **9,** 643–648 CrossRef Medline
78. Sheldrick, G. M. (2002) Macromolecular Phasing with SHELXE. *Zeitschrift für Krist.* **217,** 644–650
79. de la Fortelle, E., and Bricogne, G. (1997) Maximum-likelihood heavy-atom parameter refinement for multiple isomorphous replacement and multiwavelength anomalous diffraction methods. *Methods Enzymol.* **276,** 472–494 CrossRef Medline
80. Emsley, P., and Cowtan, K. (2004) Coot: Model-building tools for molecular graphics. *Acta Crystallogr. Sect. D Biol. Crystallogr.* **60,** 2126–2132 CrossRef Medline
81. Adams, P. D., Grosse-Kunstleve, R. W., Hung, L. W., Ioerger, T. R., McCoy, A. J., Moriarty, N. W., Read, R. J., Sacchettini, J. C., Sauter, N. K., and Terwilliger, T. C. (2002) PHENIX: Building new software for automated crystallographic structure determination. *Acta Crystallogr. D Biol. Crystallogr.* **58,** 1948–1954 CrossRef Medline
82. Smart, O. S., Womack, T. O., Flensburg, C., Keller, P., Paciorek, W., Sharff, A., Vonrhein, C., and Bricogne, G. (2012) Exploiting structure similarity in refinement: Automated NCS and target-structure restraints in BUSTER. *Acta Crystallogr. D Biol. Crystallogr.* **D68,** 368–380 CrossRef Medline
83. Painter, J., and Merritt, E. A. (2006) Optimal description of a protein structure in terms of multiple groups undergoing TLS motion. *Acta Crystallogr. D Biol. Crystallogr.* **62,** 439–450 CrossRef Medline